EPJ D
Atomic, Molecular, Optical and Plasma Physics
www.epj.org

Eur. Phys. J. D **51**, 303–312 (2009) DOI: 10.1140/epjd/e2008-00267-y

Limitations of the strong field approximation in ionization of the hydrogen atom by ultrashort pulses

D.G. Arbó, K. Tőkési and J.E. Miraglia

EDP SCIENCES
Società Italiana di Fisica
Springer

Eur. Phys. J. D **51**, 303–312 (2009)
DOI: 10.1140/epjd/e2008-00267-y

THE EUROPEAN PHYSICAL JOURNAL D

Regular Article

Limitations of the strong field approximation in ionization of the hydrogen atom by ultrashort pulses

D.G. Arbó[1], K. Tőkési[2,a], and J.E. Miraglia[1,3]

[1] Institute for Astronomy and Space Physics, IAFE, CC 67, Suc. 28 (1428) Buenos Aires, Argentina
[2] Institute of Nuclear Research of the Hungarian Academy of Science, ATOMKI, P.O. Box 51, 4001 Debrecen, Hungary
[3] Department of Physics, FCEN, University of Buenos Aires, Argentina

Received 30 September 2008
Published online 20 December 2008 –

Abstract. We present a theoretical study of the ionization of hydrogen atoms as a result of the interaction with an ultrashort external electric field. Doubly-differential momentum distributions and angular momentum distributions of ejected electrons calculated in the framework of the Coulomb-Volkov and strong field approximations, as well as classical calculations are compared with the exact solution of the time dependent Schrödinger equation. We show that in the impulsive limit, the Coulomb-Volkov distorted wave theory reproduces the exact solution. The validity of the strong field approximation is probed both classically and quantum mechanically. We found that classical mechanics describes the proper quantum momentum distributions of the ejected electrons right after a sudden momentum transfer, however pronounced the differences at latter stages that arise during the subsequent electron-nucleus interaction. Although the classical calculations reproduce the quantum momentum distributions, it fails to describe properly the angular momentum distributions, even in the limit of strong fields. The origin of this failure can be attributed to the difference between quantum and classical initial spatial distributions.

PACS. 32.80.-t Photoionization and excitation – 32.80.Fb Photoionization of atoms and ions – 42.50.Hz Strong-field excitation of optical transitions in quantum systems; multiphoton processes; dynamic Stark shift

1 Introduction

The time-dependent distorted Coulomb-Volkov approximation (CVA) has been widely used to describe the ionization processes of various atomic targets interacting with short laser pulses in the last decade [1–3]. The CVA is a time-dependent distorted-wave theory [4–6] that includes the effect of the remaining core into the final state at the same approximation level as the external field. In this way, the collision dynamics due to the effects of the core potential to the detached electron can be directly probed. Especially, CVA gains importance in those cases where the time-dependent Schrödinger equation becomes impractical to solve, at high intensities and long pulse durations, for instance. Several studies have been performed so far to determine the accuracy of the CVA, within different levels of approximations when they calculate the emission spectra for short pulses but of finite durations [7,8].

In the last two decades there has been also a great revival of the classical trajectory Monte Carlo (CTMC) calculations applied to atomic collisions involving three or more particles [9]. This approximation seems to be useful in treating atomic collisions where the quantum mechanical calculations become very complicated or intractable, which is the case usually when higher order perturbations should be applied or many particles take part in the processes [10,11]. The CTMC method has been quite successful also in dealing with the ionization process in laser-atom collisions when, instead of charged particles, electromagnetic fields are used for excitation of the target [12,13].

In the present work we study the efficiency of the strong field approximation (SFA) within the quantum CVA and the classical trajectory Monte Carlo (CTMC) method to describe the electron emission spectra of a hydrogen atom when it is excited by ultra-short pulses. The effect of a short pulse on one atom can be treated within the framework of a sudden momentum transfer (or kick) where the pulse duration is much less than the classical orbital period of the electron in the initial state [14,15]. We apply the CVA for the determination of the doubly-differential electron momentum distribution and the final angular momentum for the case of hydrogen ionization by an ultrashort electric pulse. We analytically prove that in the limit of zero pulse duration and finite momentum transfer, CVA reproduces the exact quantum mechanical electron yields. We show that CTMC method provides

[a] e-mail: tokesi@atomki.hu

accurate electron momentum distributions but not angular momentum distributions, even at the limit of strong fields.

The paper is organized as follows: in Section 2.1 we introduce the CVA as a time-dependent distorted wave theory and demonstrate that it provides for exact transition probabilities to continuum states in the case of an atom subject to a sudden momentum transfer. We briefly describe the CVA in its various versions, like (i) the sudden Coulomb-Volkov (SCV) approximation, (ii) the single-distorted approximation (SD), and (iii) the doubly-distorted (DD) approximation. Furthermore, we discuss the limitations of the well-known strong-field approximation (SFA) also denominated in the literature Keldysh-Faisal-Reiss or simply Volkov theory [16]. In Section 2.2 we shortly introduce the classical trajectory Monte Carlo (CTMC) method where the Hamilton's equations of motion of the electron are solved. We present a derivation of the relation between the angular momentum distribution and the initial spatial distribution of the electron within the SFA. In Section 3, we compare results for the quantum doubly-differential momentum distributions to classical ones. We complete the chapter with a thorough study of the classical angular momentum distributions and quantum partial populations. At the end, in Section 4 we present the conclusions. Atomic units are used throughout the paper.

2 Theory

The total Hamiltonian of a target hydrogen atom interacting with an ultrashort pulse in the dipole approximation is

$$H(t) = H_0 + V(t), \tag{1}$$

where $H_0 = \mathbf{p}^2/2 - Z/r$ is the atomic Hamiltonian, Z is the atomic charge ($Z = 1$ for the case of the hydrogen atom), $\mathbf{p}$ and $\mathbf{r}$ are the momentum and position of the electron, respectively, and $V(t) = \mathbf{r} \cdot \mathbf{F}(t)$ is the interaction term with the external electric field $\mathbf{F}(t)$ in the gauge length. For convenience, we model the external electric field as a square pulse of duration τ, by

$$\mathbf{F}(t) = -\Delta p \; \delta_\tau(t) \; \hat{\mathbf{z}} \; , \tag{2}$$

where $\delta_\tau(t)$ is any function that approaches the Dirac $\delta(t)$ in the limit of ultrashort interaction time, i.e., $\lim_{\tau \to 0} \delta_\tau(t) = \delta(t)$. For practical purposes and in order to simplify our calculations, we model the pulse shape as $\delta_\tau(t) = 1/\tau \; \Theta(\tau/2 - |t|)$. We can understand the limit $\tau \to 0$ as the pulse duration to be much shorter than the orbital time of the initial atomic state. In equation (2) the electric field defines the $\hat{\mathbf{z}}$ direction, the minus sign stems from the electron charge, and Δp is the momentum transferred to the electron. We confine our study to a hydrogen atom initially in its ground state. We calculate the momentum distribution of ejected electrons by solving the quantum and classical equations of motion as explained below.

2.1 Time-dependent distorted-wave methods

As a consequence of the interaction with the laser pulse, the electron, initially bound to the target nucleus in the state $|\phi_i\rangle$, is emitted with momentum $\mathbf{k}$ and energy $\varepsilon_f = k^2/2$. The process presents cylindrical symmetry around the direction of the electric field (polarization axis). Electron momentum distributions can be calculated from the transition matrix as

$$\frac{dP}{d\mathbf{k}} = |T_{if}|^2 \, , \tag{3}$$

where T_{if} is the T-matrix element corresponding to the transition $\phi_i \to \phi_f$, and $|\phi_f\rangle$ is the final unperturbed state.

Within the CVA, T_{if} can be computed using three different methods, namely (i) within the framework of the sudden Coulomb-Volkov (SCV); (ii) the single distorted (SD), and (iii) the doubly distorted (DD) approximations. We also discuss the strong field approximation (SFA), as a variant of the CVA [17,18].

2.1.1 Sudden Coulomb-Volkov approximation

In general, the transition amplitude in the prior form at the sudden limit is given by [5,7]

$$T_{if}^{\mathrm{SCV}} = \lim_{t \to -\infty} \langle \chi_f^{\mathrm{CV}-}(t) \, | \phi_i(t) \rangle, \tag{4}$$

where the final Coulomb-Volkov distorted-wave function $\chi_f^{CV-}(t)$ can be written as [7]

$$\chi_f^{\mathrm{CV}-}(\mathbf{r}, t) = \phi_{\mathbf{k}}^-(\mathbf{r}, t) \exp(iD^-(\mathbf{k}, \mathbf{r}, t)). \tag{5}$$

In equation (5), $\phi_{\mathbf{k}}^-$ is the unperturbed final state given by

$$\phi_{\mathbf{k}}^-(\mathbf{r}, t) = \mathrm{e}^{-i\frac{k^2}{2}t} \frac{\exp(i\mathbf{k} \cdot \mathbf{r})}{(2\pi)^{3/2}} \; \mathcal{D}_C(Z, \mathbf{k}, t), \tag{6}$$

where $\mathcal{D}_C(Z, \mathbf{k}, t) = N_T^-(k) \; {}_1F_1(-iZ/k, 1, -ikr - i\mathbf{k} \cdot \mathbf{r})$. The Coulomb normalization factor $N_T^-(k) = \exp(\pi Z/2k) \; \Gamma(1 + iZ/k)$ is the value of the Coulomb wave function at the origin ($\mathbf{r} = \mathbf{0}$), and ${}_1F_1$ denotes the confluent hypergeometric function. The Volkov phase D^- in equation (5) is given by [19]

$$D^{\pm}(\mathbf{k}, \mathbf{r}, t) = \mathbf{A}^{\pm}(t) \cdot \mathbf{r} - \mathbf{k} \cdot \int_{\mp\infty}^{t} dt' \; \mathbf{A}^{\pm}(t') - \frac{1}{2} \int_{\mp\infty}^{t} dt' \; \left(\mathbf{A}^{\pm}(t')\right)^2 , \tag{7}$$

where $\mathbf{A}^{\pm}(t) = -\int_{\mp\infty}^{t} dt' \; \mathbf{F}(t')$ is the vector potential. The wave functions $\phi_i(t)$ and $\phi_{\mathbf{k}}^-(t)$ are solutions of

the time dependent Schrödinger equation with the non-perturbed Hamiltonian:

$$i\frac{\partial}{\partial t}|\phi_i(t)\rangle = H_0|\phi_i(t)\rangle = \varepsilon_i|\phi_i\rangle \tag{8a}$$

$$i\frac{\partial}{\partial t}|\phi^-_{\mathbf{k}}(t)\rangle = H_0|\phi^-_{\mathbf{k}}(t)\rangle = (k^2/2)|\phi^-_{\mathbf{k}}(t)\rangle. \tag{8b}$$

In particular, for the case of the square pulse of equation (2), the vector potential reduces to $\mathbf{A}^{\pm}(t) = \mathbf{\Delta p}\,(1/2 \pm t/\tau)$ for $-\tau/2 \le t \le \tau/2$, and equation (7) becomes a close form

$$D^{\pm}(\mathbf{k},\mathbf{r},t) = \mathbf{\Delta p}\,(t/\tau \pm 1/2)\cdot\mathbf{r} - \mathbf{k}\cdot\frac{\mathbf{\Delta p}}{2}\tau\ (t/\tau\pm 1/2)^2 + \frac{|\mathbf{\Delta p}|^2}{6}\tau\,(t\pm\tau/2)^3\,. \tag{9}$$

when $-\tau/2 \le t \le \tau/2$.

Replacing equation (9) into the final distorted wave function of equation (5) and this into equation (4), the SCV transition probability (Eq. (3)) becomes

$$\left(\frac{dP}{d\mathbf{k}}\right)^{\mathrm{SCV}} = |T_{if}^{\mathrm{SCV}}|^2 = \left|\langle\phi^-_{\mathbf{k}}(\mathbf{r})\right| e^{i\mathbf{\Delta p}\cdot\mathbf{r}}\ \left|\phi_i(t)\right\rangle\right|^2, \tag{10}$$

which results equal to the exact quantum transition probability when the external field is reduced to a sudden momentum transfer of strength $\mathbf{\Delta p} = -\int_{-\infty}^{\infty} dt\ \mathbf{F}(t)$ [14]. The second and third terms of the Volkov phase D^- in equation (7) do not contribute to the transition probability since they do not depend on the electron position $\mathbf{r}$ and, therefore, add only a time dependent phase to the transition amplitude which is cancelled out by the absolute value in equation (10). Hence, the SCV describes the exact quantum transition probability in the sudden limit, i.e., $\tau \to 0$. This means the SCV reckons the interaction of finite duration between the electron and the external field as a sudden momentum transfer localized at a particular time (in this case $t = 0$).

2.1.2 Single distorted approximation

The transition amplitude in the post form within the SD approximation can be expressed as [5]

$$T_{if}^{\mathrm{SD}+} = -i\int_{-\infty}^{+\infty} dt\ \langle\chi_f^{\mathrm{CV}-}(t)|V(t)\,|\phi_i(t)\rangle. \tag{11}$$

One could be tempted to directly calculate the Volkov phase shift for sudden momentum transfer as $D^{\pm}(\mathbf{k},\mathbf{r},0^{\pm}) = \lim_{\tau\to 0} D^{\pm}(\mathbf{k},\mathbf{r},t) = \pm\mathbf{\Delta p}\cdot\mathbf{r}$ and then to solve the time integral by making use of the temporal delta function originating from the potential $V(t)$ in equations (2), but this would lead to incorrect transition probabilities due to the improper handling of the time limits for ultra short pulses in equations (11) and (2). The correct way to derive $T_{if}^{\mathrm{SD}+}$ for a sudden momentum transfer is to perform the whole calculation for a short (but finite) pulse of duration τ and then, at the end, take the limit of $\tau \to 0$. In the case of the square field of equation (2), the Volkov phase is described by equation (9). The second and third terms on the right hand side of equation (9) are of the same order: $O(\tau)$, while the first term is $O(\tau^0)$. Therefore, we preserve only the term which depends on the spatial coordinates in our calculations and consequently equation (11) becomes

$$T_{if}^{\mathrm{SD}+} = \frac{i}{\tau}\ \langle\phi^-_{\mathbf{k}}(\mathbf{r})|\mathbf{\Delta p}\cdot\mathbf{r}\ e^{i\mathbf{\Delta p}\cdot\mathbf{r}/2}\,I(\mathbf{\Delta p}\cdot\mathbf{r})\,|\phi_i(t)\rangle, \tag{12}$$

where we have exchanged the order of spatial and time integrals reducing, in this way, the temporal integral to the factor $I(\mathbf{\Delta p}\cdot\mathbf{r})$ given by $I(x) = \int_{-\tau/2}^{+\tau/2} dt\ e^{-itx/\tau} = 2\tau\sin(x/2)/x$. In equation (12) we have also neglected the factor $\exp(i\varepsilon_i t)$ resulting from the time evolution of the initial state since the exponent is also of the same order as $O(\tau)$ in equation (9). Considering the orthogonality condition between the initial and final states, the SD transition amplitude reduces again to the exact result

$$T_{if}^{\mathrm{SD}+} = \langle\phi^-_{\mathbf{k}}(\mathbf{r})|e^{i\mathbf{\Delta p}\cdot\mathbf{r}}\,|\phi_i(t)\rangle. \tag{13}$$

It is important to recall that we use the orthogonality condition; if approximated continuum wave functions are used the equality in the sudden limit is violated.

2.1.3 Doubly distorted approximation

In the doubly-distorted (DD) CVA, the transition amplitude is calculated distorting both initial and final states [5]

$$T_{if}^{\mathrm{DD}} = T_{if}^{\mathrm{SCV}} - i\int_{-\infty}^{+\infty} dt\ \langle\chi_f^{\mathrm{CV}-}(t)|W_i(t)\left|\chi_i^{\mathrm{CV}+}(t)\right\rangle, \tag{14}$$

where T_{if}^{SCV} is the transition amplitude in the SCV approximation given in equation (4) and the initial Coulomb-Volkov distorted wave function reads as

$$\chi_i^{\mathrm{CV}+}(\mathbf{r},t) = \phi_i(\mathbf{r},t)\exp(iD^+(\mathbf{0},\mathbf{r},t)). \tag{15}$$

The operator $W_i(t)$ in equation (14) acts on the distorted initial state in the following way

$$W_i(t)\chi_i^{\mathrm{CV}+}(t) = -i\nabla\phi_i(\mathbf{r},t)\cdot A^+(t)\ \exp[iD^+(\mathbf{0},\mathbf{r},t)]. \tag{16}$$

The time domain of the external field for the same square finite field described in equation (2) is $-\tau/2 \le t \le \tau/2$, thus, the limits of the integral in second term of equation (14) should keep within these values. Then, as the integrand in equation (14) is finite and does not diverge in the limit $\tau \to 0$, the whole integral in equation (14) vanishes. Therefore, the DD transition amplitude collapses to the SCV one in the limit of sudden momentum transfers, i.e., $T_{if}^{\mathrm{DD}} = T_{if}^{\mathrm{SCV}}$.

In summary, by calculating the transition probability produced by an ultrashort pulse in the sudden limit (sudden momentum transfer, i.e., $\tau \to 0$), through any of the above mentioned versions of the CVA -sudden Coulomb-Volkov (SCV), single distorted (SD), or double distorted (DD), we obtain the same result as by solving the TDSE exactly, i.e., $T_{if}^{SCV} = T_{if}^{SD} = T_{if}^{DD} = T_{if}^{TDSE}$, where we T_{if}^{TDSE} is the exact quantum mechanical transition probability.

For the sake of completeness, we mention that the first Born approximation can be calculated within the SD version of the CVA by inserting the final state $\phi_{\mathbf{k}}^{-}(\mathbf{r})$ instead of the distorted Coulomb-Volkov wave function $\chi_f^{CV-}(t)$ into equation (11). This results in the dipole approximation of the transition matrix

$$T_{if}^{1B} = i\ \mathbf{\Delta p} \cdot \langle \phi_{\mathbf{k}}^{-}(\mathbf{r}) | \mathbf{r}\, | \phi_i(t) \rangle, \tag{17}$$

which is valid when the external field can be described only perturbatively, i.e., $\mathbf{\Delta p} \cdot \mathbf{r} \ll 1$.

2.2 Classical simulation in the sudden limit

The classical trajectory Monte Carlo method (CTMC) is a non-perturbative method, where classical equations of motion are solved numerically. The microcanonical ensemble that characterizes the initial state of the target is here assumed as:

$$\rho_{E_0}(\mathbf{r}, \dot{\mathbf{r}}) = C_1 \delta(E_0 - E) = C_1 \delta \left(E_0 - \frac{1}{2}\dot{\mathbf{r}}^2 - V(r) \right), \tag{18}$$

where C_1 is a normalization constant, E_0 is the binding energy of the active electron and $V(r)$ is the electron and target-core potential. According to the equation (18), the electronic coordinate is confined to the intervals where the relation

$$\frac{\dot{\mathbf{r}}^2}{2} = E_0 - V(r) > 0 \tag{19}$$

is verified.

In the present CTMC approach, Hamilton's classical nonrelativistic equations of motion are solved [10,20,21] numerically when an external field is taken into account as a kick. The solutions of the Hamilton's equations during the kick reduces to a shift Δp along the $\hat{z}$ component of the momentum of the initial distribution in phase space. For the ionization channel the final energy and the scattering angles (polar and azimuth) of the projectile and the ionized electron were recorded. These parameters were calculated at large separations of the ionized electron and the target nucleus, where the Coulomb interaction is negligible. The double differential ionization probability (P_i) was computed with the following formula:

$$P_i = \frac{d^2P}{dk_\rho dk_z} = \frac{N_i}{N \Delta k_\rho \Delta k_z}, \tag{20}$$

while the angular momentum distribution is calculated by means of:

$$P_i = \frac{dP}{dL} = \frac{N_i}{N \Delta L}. \tag{21}$$

The standard deviation for a differential probability is defined through:

$$\Delta P_i = P_i \left[\frac{N - N_i}{N N_i} \right]^{1/2}. \tag{22}$$

In equations (20)–(22) N is the total number of classical trajectories calculated for the given collision system, N_i is the number of trajectories that satisfy the criteria for ionization under consideration in the perpendicular momentum interval (or box dimension) Δk_ρ and the parallel momentum interval Δk_z, or in the angular momentum interval ΔL of the electron.

2.3 Quantum and classical strong field approximations

The strong field approximation assumes that the electron is driven only by the strong external electric field and neglects the Coulomb attraction of its nucleus in the final state. Similarly, from the mathematical point of view, SFA reduces to the replacement of $\mathcal{D}_C(Z_T, \mathbf{k}, t)$ by 1 in equation (6). This means that the final state is represented as a pure Volkov state [19] and not as a Coulomb-Volkov wave function as in equation (5). Hence, the total transition probability by a sudden momentum transfer of strength $\mathbf{\Delta p}$ within the SFA is the simple Fourier transform of the initial wave function shifted by the magnitude $\mathbf{\Delta p}$ in the momentum space

$$\frac{dP^{\mathrm{SFA}}}{d\mathbf{k}} = \left| \tilde{\phi}_i(\mathbf{k} - \mathbf{\Delta p}) \right|^2, \tag{23}$$

where $\tilde{\phi}_i$ denotes the Fourier transform of the initial state ϕ_i. For the case of the hydrogen atom in cylindrical coordinates it reads

$$\frac{dP^{\mathrm{SFA}}}{dk_\rho dk_z} = k_\rho \frac{16/\pi}{[1 + k_\rho^2 + (k_z - \Delta p)^2]^4}. \tag{24}$$

Considering the Parseval-Plancherel theorem which states that a function and its Fourier transform have the same norm, it turns out that the total ionization probability within the SFA is equal to unity. This result does not depend on the value of $\mathbf{\Delta p}$, which shows the proper limit of the SFA for strong kicks ($\mathbf{\Delta p} \gg 1$) and it also gives incorrect results when $\mathbf{\Delta p}$ is small or even zero! This is due to the lack of orthogonality between the initial and final states. As the SFA neglects the effect of the Coulomb potential on the electron after the kick, it predicts the exact velocity distribution of the electron yield right after the kick, at $t = 0^+$, when no further Coulomb attraction is possible yet. A direct comparison of CVA and SFA results lets us study the effect of the Coulomb potential on the momentum of the escaping electron, which is exactly calculated in the full CVA but completely neglected in the SFA. In the perturbative limit, the SFA predictions of the final momentum distributions and total ionization probabilities are completely wrong, as previously mentioned.

However, the SFA transition probability $dP^{\rm SFA}/d\mathbf{k}$ calculated in equation (23) as a shift $\mathbf{\Delta p}$ of the Fourier transform of the initial wave function does provide the exact electron momentum (or velocity) distribution right after the sudden momentum transfer (at $t = 0^+$). As seen from equation (23), this is only a shift $\mathbf{\Delta p}$ of the initial electron momentum distribution.

In the SFA, the classical momentum distribution is not affected by the Coulomb potential. As both classical and quantum results of the SFA are reduced to a shift $\mathbf{\Delta p}$ in momentum and as the CTMC initial momentum distribution in the microcanonical ensemble perfectly replicates the quantum one, the final classical and quantum momentum distributions are the same within the SFA, which is a good approximation for the case of $\Delta p \gg 1$. The width of the SFA electron momentum distribution is unaffected by the kick. Thus, the relative ratio of the momentum distribution width relative to the displacement Δp diminishes as the kick strength increases. In consequence, we can consider an additional approximation (peaking approximation) in which the whole momentum distribution after the kick concentrates at $\mathbf{k} = \mathbf{\Delta p}$, i.e., $dP/d\mathbf{k} = \delta(\mathbf{k} - \mathbf{\Delta p})$. In this case, the absolute value of the angular momentum can be simply written as $L = \rho\Delta p$, where ρ is the radial cylindrical coordinate. Therefore, the classical angular momentum distribution can be derived directly from the initial radial momentum distribution via the simple relation

$$\frac{dP}{dL} = \frac{1}{\Delta p}\frac{dP}{d\rho}. \tag{25}$$

For the current case of sudden momentum transfer the initial and final distributions in position space are the same, thus, as the initial ρ-distribution is known, one can replace $\rho = L/\Delta p$ on the right half side of equation (25) and, in this way, the final angular momentum distributions can be obtained.

When using the microcanonical ensemble for the initial CTMC distributions, the cylindrical radial distribution for the ground state reads $dP^{\rm C}/d\rho = -3Z^3\rho(\rho - 2/Z)/4$. Now, by using equation (25), the final classical angular momentum distribution within the SFA results can be written as:

$$\frac{dP}{dL}^{\rm SFA-C} = \frac{-3Z^3}{4(\Delta p)^3}L(L - 2\Delta p/Z). \tag{26}$$

As expected for the case of the SFA, the integral of equation (26) over all possible values of L is equal to 1, which indicates that the atom is fully ionized.

Along this line, we can ask what the relation between the initial ρ-distribution and the final partial populations p_l in quantum mechanics is. The difficulty stems from the discreteness of the absolute value of the angular momentum. But, considering that in the SFA $\Delta p \gg 1$ and the average value of the cylindrical radial coordinate ρ is of the order of the unity, we can say that the angular momentum (on average) is much higher than the step size between consecutive angular momentum values, which is of the order of 1. Hence, it is a good approximation, within the SFA, to consider the quantum angular momentum and the quantum orbital number as a continuum variable. Consequently, the relation between the initial distribution in spatial coordinates and the final partial populations preserves in quantum mechanics.

In quantum mechanics the initial spatial distribution is given by the square of the absolute value of the initial wave function. In the case of the ground state of the hydrogen atom the initial ρ-distribution, calculated by results after integrating over the remaining cylindrical coordinates, can be written as $dP^{\rm Q}/d\rho = 4Z^3\rho^2K_1(2Z\rho)$, where K_1 is the modified Bessel function of second kind. With the help of equation (25), we calculate the quantum final partial populations (or angular momentum distribution) within the SFA, which reads

$$\frac{dP}{dL}^{\rm SFA-Q} = \frac{4Z^3L^2}{(\Delta p)^3}K_1(2ZL/\Delta p). \tag{27}$$

Analogously to the classical case, the integral over all possible values of L is 1 indicating the total atomic ionization. A thorough comparison between the quantum SFA momentum distributions and the full quantum (CVA) needs to establish a relation between the classical angular momentum L and the orbital quantum number l. As we will show below, the prescription widely used in the literature $L = l + 1/2$ seems to be adequate.

We can derive the most probable classical and quantum angular momentum within the SFA by finding the maxima of angular momentum distributions in equations (26) and (27), respectively. For the quantum case the most probable angular momentum within SFA is $L_0^{\rm SFA-Q} \simeq 0.67\Delta p/Z$, while the classical most probable angular momentum within SFA is $L_0^{\rm SFA-C} = \Delta p/Z$ and there is a cut-off at the double, i.e., $2\Delta p/Z$. For high momentum transfers (SFA) the influence of the Coulomb field is neglected and only the difference in the initial conditions are responsible for the difference of the classical and quantum angular momentum distributions. No limit is found at high kick strengths so that the quantum and classical angular momentum distributions coincide, in opposition to extended oscillatory pulses where quantum-classical correspondence is found for near-threshold tunneling ionization [22].

3 Results and discussion

3.1 Doubly-differential momentum distribution

It is a well-known fact that in the case of the low kick strengths (dipole or perturbative regime), quantum and classical dynamics for the ionization yield of a hydrogen atom predict very different outcomes. For example, for ionization of a hydrogen atom due to a sudden momentum transfer $\Delta p = 0.25$ whereas quantum mechanics 2%, CTMC predicts only 0.4%, which is five times lower. This behavior is called in the literature classical suppression [14]. But not only the total ionization probability is underestimated by classical calculations, differential momentum distributions also look different. In Figure 1 the

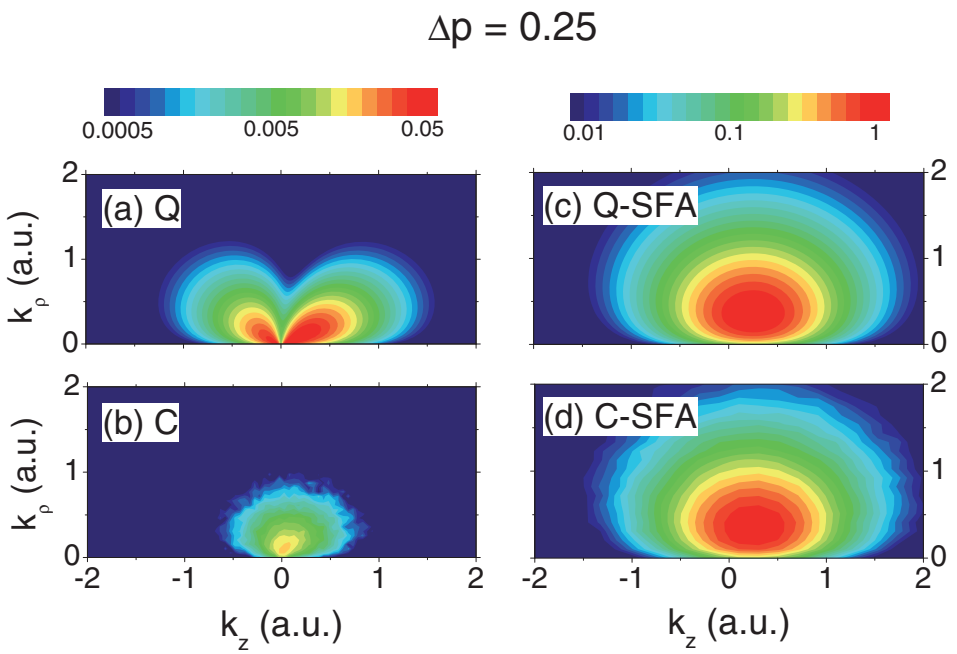

Fig. 1. (Color online) Doubly-differential electron momentum distributions (logarithmic scale) in cylindrical coordinates (k_z, k_ρ). First row (a) and (c): quantum results, second row (b) and (d): classical results. First column (a) and (b): exact, second column (c) and (d): SFA. The momentum transfer is $\Delta p = 0.25$.

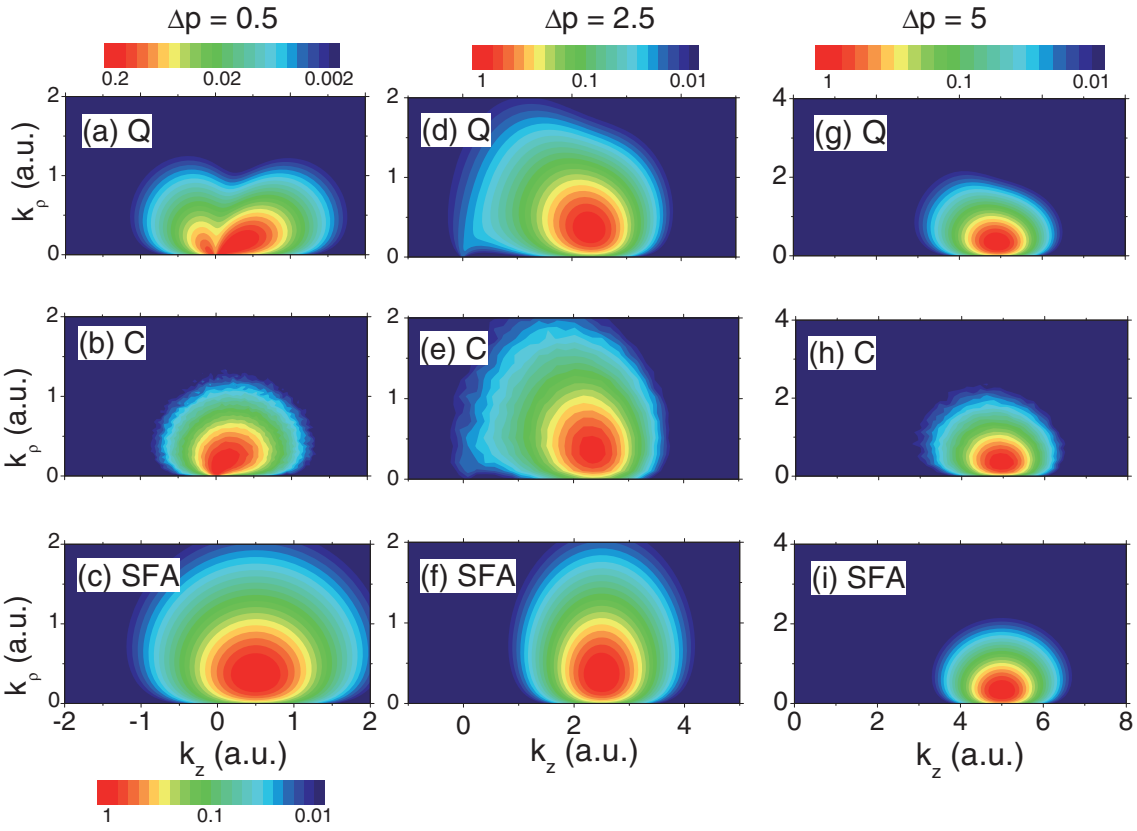

Fig. 2. (Color online) Doubly-differential electron momentum distributions (logarithmic scale) in cylindrical coordinates (k_z, k_ρ). First row (a), (d), and (g): quantum; second row (b), (e), and (h): classical; and third row (c), (f), and (i): SFA. The momentum transfer is $\Delta p = 0.5$, 2.5, and 5 for the first ((a), (b), and (c)), second ((d), (e), and (f)), and third ((g), (h), (i)) column, respectively.

quantal (Fig. 1a) and classical (Fig. 1b) doubly-differential momentum distribution $d^2P/dk_\rho dk_z$ of the electron yield after a sudden momentum transfer of strength $\Delta p = 0.25$ are displayed. We note that the grey (color on line) coding is in the same logarithmic scale. While the quantal distribution shows two lobes (Fig. 1a), the classical one does not reproduce this quantal behavior and shows only one lobe (Fig. 1b) slightly tilted towards the forward direction (in the direction of the kick). In the case of the quantum distribution the right lobe (direction of the momentum transfer, $\mathbf{\Delta p}$) is bigger than the left lobe (opposite direction), and therefore the average final momentum of the electron is positive, as expected. The two quantum lobes are related to the dipole transition elements.

Figure 1c shows the SFA doubly-differential momentum distribution calculated quantum mechanically through equations (23) and (24). The distribution exhibits only one spot in the direction of the kick, evidencing no traces of dipole transitions. The average SFA momentum (center of the spot) is at $k_z = \Delta p = 0.25$. Figure 1d show the corresponding classical momentum distribution right after the kick. We note that both quantum and classical SFA momentum distributions look the same within the statistical errors in CTMC values (below 0.05 a.u.), which are about 8% due to the finite number of the analyzed primary trajectories. A direct comparison of Figures 1c and 1d not only shows that within the SFA the time evolutions of a classical and quantum sudden momentum transfer are exactly the same, i.e., classical dynamics has exactly the same ionization yield as quantum mechanics, but also that the dynamics of a sudden momentum transfer is equally described by the time dependent Schrödinger equation and the Hamilton equations. Nevertheless, the time evolution of the motion of the kicked electron under the effect of the atomic Coulombic electric field shows significant differences, which is confirmed in Figures 1a and 1b, where the final electron distributions are shown. In the following figures only the SFA results calculated in the framework of the CVA, free from any statistical error, are shown.

As the kick strength increases, the total classical ionization probability tends to the quantum one. For $\Delta p = 0.5$ and 2.5 the total classical ionization probabilities are 7.7%, and 96.1%, respectively, while the quantum ones are 9.6% and 96.8%, respectively. At $\Delta p = 5$ both formalisms predict almost full ionization i.e. $\sim 100\%$. We follow the doubly differential momentum distribution when the kick strength changes from the dipole ($\Delta p \ll 1$) to the SFA ($\Delta p \gg 1$) regime, as can be seen in Figures 2a–2c, Figures 2d–2f and Figures 2g–2i, for $\Delta p = 0.5$, 2.5 and 5, respectively. We show in Figure 2 the quantum (top), classical (medium), and SFA (bottom) results. The three doubly-differential momentum distributions in Figures 2g–2i look practically indistinguishable. In Figure 2a the lobe in the forward direction of the quantum momentum distribution is much bigger than the one in the backward direction, indicating that we are moving away from the dipole limit. Figure 2b shows that the classical momentum distribution starts to be like the quantum mechanical forward lobe, but still, for this low kick strength, differences are significant. The SFA momentum distribution in Figure 2c is centered at $k_z = \Delta p$ and is quite different from quantal and classical momentum distributions of Figures 2a and 2b, which shows that ionization by a kick of $\Delta p = 0.5$ is far from the strong field regime. Since Figure 2c displays the velocity distribution right after the kicks (SFA), a direct comparison between Figures 2a and 2b show the strong effect of the atomic Coulomb potential on escaping electrons after weak kicks. We note that the discrepancies in the quantum and classical momentum distributions can be due to two different effects: (i) the difference in the quantum and classical time evolution operator of the electron under the influence of the Coulomb potential and (ii) the difference in the initial conditions in the phase space. In particular, as the quantum and classical momentum distributions coincide, the differences mentioned in (ii) reside in the position coordinates.

For a kick of strength $\Delta p = 2.5$ quantum-classical correspondence is observed not only in the total ionization yield but also in the doubly-differential momentum distributions (see Figs. 2d and 2e). Quantum mechanics brings in only one lobe (see Fig. 2d) in the forward direction which can be accurately reproduced by classical mechanics. The right lobe observed for weak kicks (see Fig. 2a) disappears as we are far away from the dipole regime. When we compare it to that of the SFA result (see Fig. 2f) we observe an overall agreement. However, essentially two differences arise: (i) the center of the full quantum and classical distributions of Figures 2a and 2b (most probable z component of the momentum) are slightly shifted towards the origin with respect to the SFA, which is exactly at $k_z = \Delta p = 2.5$, and (ii) the full quantum and classical momentum distributions are weakly distorted near the origin ($\mathbf{k} = \mathbf{0}$) due to the effect of the Coulomb field. This near-threshold distortion is obviously not present in the SFA momentum distribution (see Fig. 2f). We show in Figures 2g–2i that for a kick strength of $\Delta p = 5$ the strong field regime is reached.

3.2 Angular momentum analysis

In this section we investigate the angular momentum of electrons emitted from the hydrogen atom by the action of the external sudden momentum transfer $\mathbf{\Delta p}$. In Figure 3 we show the partial quantum populations p_l and compare it to the continuum classical angular momentum distribution dP/dL as a function of the orbital quantum number l and the angular momentum L, respectively. As it is known, near the dipole limit (small Δp), quantum mechanics predicts the population of p states only (see Figs. 3a and 3b). In turn, classical dynamics predicts angular momenta below $L = 1$ for weak kicks as shown in Figure 3a. But, for a kick strength $\Delta p = 0.5$ classical and quantal curves, despite the intrinsic difference in their continuity and discreetness, look quite alike. As we will immediately see, this is not related to any classical-quantum correspondence but it is a fortuitous fact. When kick strengths are increased, the quantum and

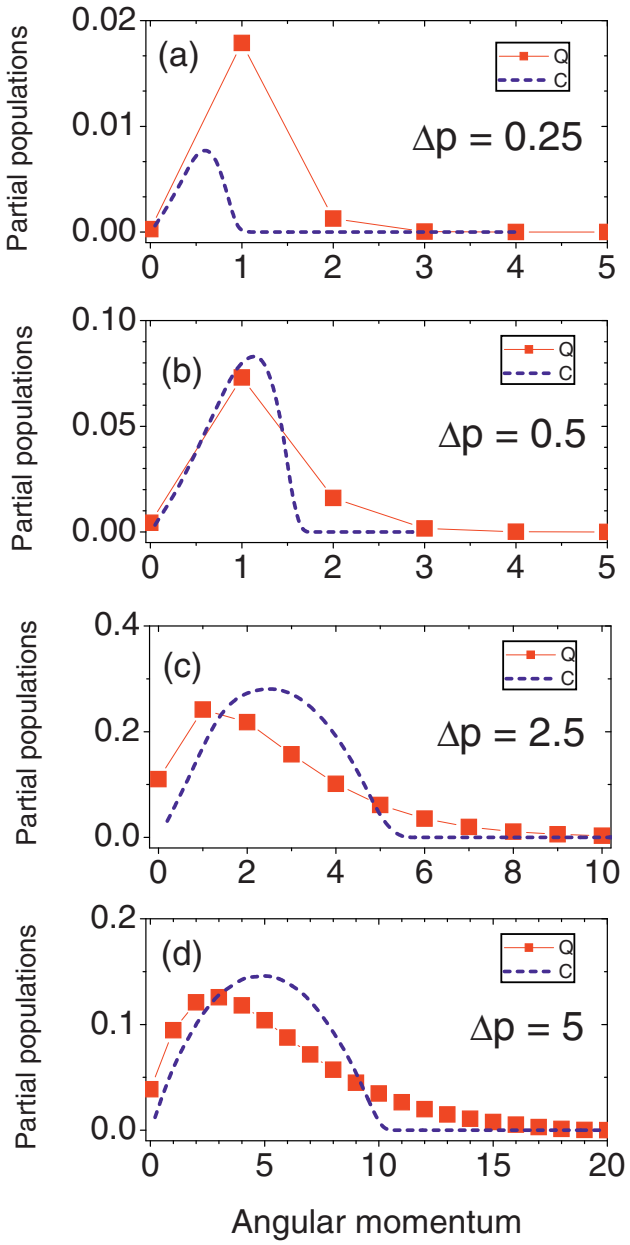

Fig. 3. (Color online) Partial wave populations p_l as a function of the orbital number l (dotted line) and angular momentum distribution of classical trajectories (Eq. (21)) (dashed line). Lines connecting the dots are included only for eye guidance. The momentum transfer is (a) $\Delta p = 0.25$, (b) $\Delta p = 0.5$, (c) $\Delta p = 2.5$, and (d) $\Delta p = 5$.

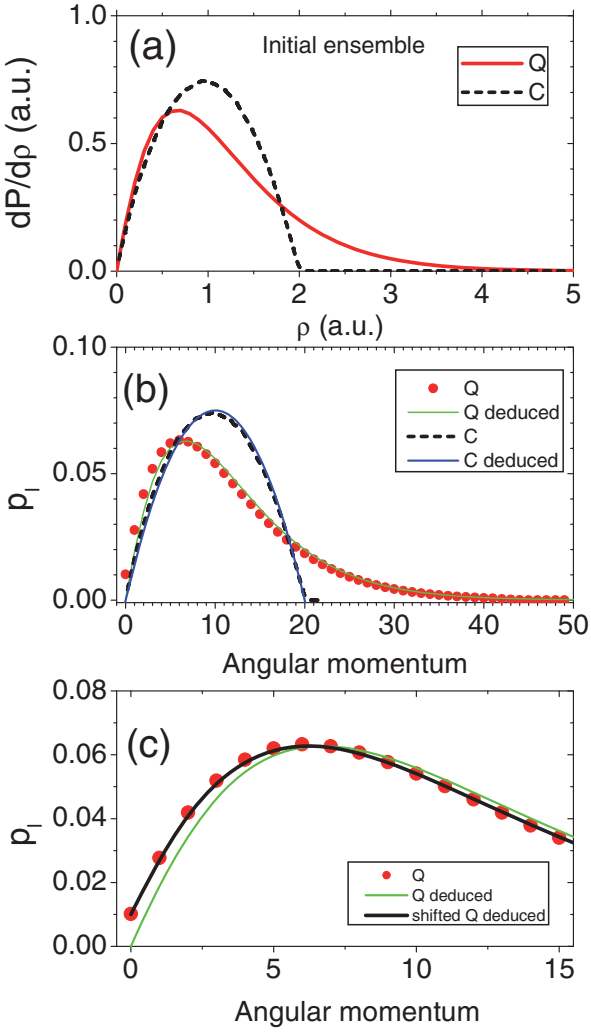

Fig. 4. (Color online) (a) Distribution of the initial state $dP/d\rho$ as a function of the radial cylindrical coordinate. Full red line is the quantum distribution and dotted black line the classical distribution. (b) Partial ionization probability p_l as a function of the angular momentum l (red dots) and angular momentum distribution of classical trajectories (dashed line) corresponding to atomic ionization by a kick of strength $\Delta p = 10$. Full lines correspond to quantum (green) and classical (blue) estimations given by equations (27) and (26), respectively. (c) Partial ionization probability p_l as a function of the angular momentum l as in (b) where we have added a shift of 1/2 in the angular distribution of equation (27).

classical distributions are different as shown in Figure 3c for $\Delta p = 2.5$ and Figure 3d for $\Delta p = 5$. In this case, whereas quantum partial populations are high for low angular momentum and possess a long tail for high l, classical distributions are characterized by a cut-off from which the distribution is zero and is centered at an angular momentum that is half the cut-off. These are main features of the SFA.

In Figure 4a we compare the classical and quantum radial distributions $dP/d\rho$ of the initial state mentioned in Section 2. Whereas the classical distribution exhibits a cutoff at $\rho = 2Z^{-1}$ and a maximum at $\rho = Z^{-1}$, the quantum radial distribution (stemming from the square of the absolute value of the wave function) possesses a long tail for high ρ and a maximum at $\rho \simeq 0.7$. In Figure 4b the final classical and quantum angular momentum distributions are shown after the interaction with a kick of strength $\Delta p = 10$. As expected from equation (25), angular momentum distributions show the same characteristic as the initial cylindrical radial distributions. We show an

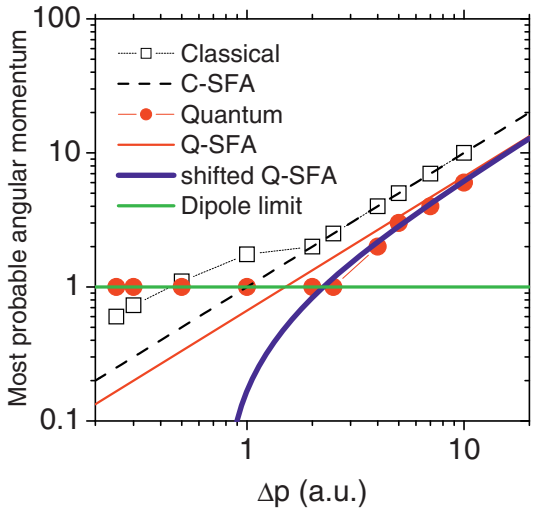

Fig. 5. (Color online) Quantum (red circular dots) and classical (empty square dots) most probable angular momentum of emitted electrons as a function of the kick strength Δp. Dots corresponding to calculations are connected with straight lines. Quantum and classical SFA predictions are shown in full red and dashed black lines, respectively. Shifted quantum SFA prediction is also shown in blue.

excellent agreement with the SFA prediction both classically (Eq. (26)) and quantum mechanically (Eq. (27)). Tiny discrepancies in the classical angular momentum distribution show the statistical errors in the calculations and the use of a finite Δp, that is, small variations with respect to the SFA. The quantum populations show no cutoff but a long tail for high orbital quantum number l and the most populated partial wave correspond to $l = 6$. In Figure 4b we see that the agreement with the SFA prediction of equation (27) is very good. Opposite to the classical case, the small discrepancies for the quantum distributions are systematic; in this case there is a small horizontal displacement between the SFA estimation of equation (27) with respect to the calculated partial populations, as observed in Figure 4c. By shifting the quantum SFA angular momentum distribution of equation (27) using the prescription $L = l + 1/2$ mentioned in last section, the agreement of the quantum angular momentum distribution with its SFA estimation (Eq. (27)) is excellent (see Fig. 4c).

In Figure 5 we probe the range of validity of the SFA to predict the most probable angular momentum. We compare the most probable angular momentum calculated as the maximum of $(dP/dL)^{\mathrm{SFA-Q}}$, i.e., $L_0^{\mathrm{SFA-Q}}$ to the quantum one calculated with the full CVA (Eq. (10)). The agreement is very good for high Δp, i.e., $\Delta p > 5$. For low Δp the ejected electron possesses mostly an angular momentum $l_0 = 1$ as expected by the dipole limit. However, to make our results consistent we should shift the quantum prediction $L_0^{\mathrm{SFA-Q}}$ according to the prescription $L = l + 1/2$. We show the effect of this shift in Figure 5. The agreement to the calculated most probable angular momentum distribution improves considerably. The most probable angular momentum can now be accurately described in the whole domain of kick strengths by either the dipole approximation or the SFA. Of course, this is not extendable to the shape of the angular momentum distribution (see Fig. 3). In Figure 5, the most probable classical angular momentum within the SFA $L_0^{\mathrm{SFA-C}} = \Delta p/Z$ is compared to the full CTMC calculations as a function of the kick strength. For kick strengths $\Delta p > 2$ the SFA most probable angular momentum agrees with the full CTMC ones but for low Δp it fails to do so for two different reasons. Firstly, the size of the SFA momentum distribution is comparable to the kick strength Δp (or bigger) and the peaking approximation, i.e., $L = \rho \Delta p$ is not valid any more. Secondly, the complete ionization considered in the SFA is far from being true for $\Delta p < 2$. This figure shows a crossing between the classical and quantum most probable angular momentum curves at $\Delta p = 0.5$. For this case, as was shown in Figure 3b, the fact that CTMC correctly reproduces the quantum most probable partial populations is only fortuitous. Cohen [12] explains that for $H^+ - H$ collisions the difference between classical and quantum angular momentum can be overcome by choosing a classical radial distribution that mimics the quantum one.

4 Conclusions

We have shown that the Coulomb-Volkov approximation (CVA) describes the quantum atomic ionization probabilities exactly when the external field is described by a sudden momentum transfer. The velocity distribution of emitted electrons right after ionization by a sudden momentum transfer is given through the strong field approximation (SFA) within both the CVA and CTMC methods. In this case, the classical and quantum time dependent evolutions of an atom subject to a sudden momentum transfer are identical. The difference between the classical and quantum final momentum distributions resides in the time evolution of the escaping electron under the subsequent action of the Coulomb field. Furthermore, classical mechanics is incapable of reproducing the quantum angular momentum distribution due to the improper initial radial distribution used in the CTMC calculations, i.e., the microcanonical ensemble. We find that in the limit of high momentum transfer, based on the SFA, there is a direct relation between the cylindrical radial distribution $dP/d\rho$ and the final angular momentum distribution dP/dL. This leads to a close analytical expression for the partial wave populations $(dP/dL)^{\mathrm{SFA-Q}}$ given by equation (27) which, together with the prescription $L = l + 1/2$, reproduces quite accurately the quantum (CVA) results. Considering the inverse problem, knowing the final angular momentum distribution can lead to the inference of the initial probability distribution, and consequently, the atomic potential. The SFA prediction for the most probable partial population results to be very accurate except in the dipole regime, when $l_0 = 1$.

The authors acknowledge fruitful discussions with M.S. Gravielle. This work was performed with financial support of CONICET, UBACyT, and ANPCyT PICT 772 of Argentina, the Hungarian-Argentine collaboration PA05-EIII/007, the Bolyai grant from the Hungarian Academy of Sciences, the Hungarian National Office for Research and Technology and the Hungarian Scientific Research Found OTKA (K72172). One of us (KT) was also partially supported by the European COST Action CM0702.

References

1. F.H.M. Faisal, G. Schlegel, J. Phys. B **38**, L223 (2005)
2. D.B. Milosevic, G.G. Paulus, D. Bauer, W. Becker, J. Phys. B **39**, R203 (2006)
3. D. Bauer, D.B. Milosevic, W. Becker, J. Mod. Opt. **53**, 135 (2006)
4. D.B. Milosevic, G.G. Paulus, W. Becker, Opt. Express **11**, 1418 (2003)
5. P.A. Macri, J.E. Miraglia, M.S. Gravielle, J. Opt. Soc. Am. B **20**, 1801 (2003)
6. V.D. Rodriguez, E. Cormier, R. Gayet, Phys. Rev. A **69**, 053402 (2004)
7. G. Duchateau, E. Cormier, R. Gayet, Eur. Phys. J. D **11**, 191 (2000); G. Duchateau, E. Cormier, H. Bachau, R. Gayet, Phys. Rev. A **63**, 053411 (2001)
8. D.G. Arbó, J.E. Miraglia, M.S. Gravielle, K. Schiessl, E. Persson, J. Burgdörfer, Phys. Rev. A **77**, 013401 (2008)
9. R.E. Olson, C.O. Reinhold, D.R. Schultz, High-Energy Ion-Atom Collisions, *Proc. IVth Workshop on High-Energy Ion-Atom Collision Processes*, Debrecen, Hungary, 1990, edited by D. Berényi, G. Hock, Lect. Notes Phys. **376**, 69 (1991), references therein
10. K. Tőkési, G. Hock, Nucl. Instrum Meth. B **86**, 201 (1994)
11. K. Tőkési, G. Hock, J. Phys. B **29**, 119 (1996)
12. J.S. Cohen, J. Phys. B **18**, 1759 (1985)
13. K.I. Dimitriou, D.G. Arbó, S. Yoshida, E. Persson, J. Burgdörfer, Phys. Rev. A **70**, 061401(R) (2004)
14. C.O. Reinhold, J. Burgdörfer, J. Phys. B **26**, 3101 (1993); C.O. Reinhold, M. Melles, H. Shao, J. Burgdörfer, J. Phys. B **26**, L659 (1993)
15. D.G. Arbó, C.O. Reinhold, J. Burgdörfer, A.K. Pattanayak, C.L. Stokely, W. Zhao, J.C. Lancaster, F.B. Dunning, Phys. Rev. A **67**, 063401 (2003)
16. L.V. Keldysh, Sov. Phys. JETP **20**, 1307 (1965); F.H.M. Faisal, J. Phys. B **6**, L89 (1973); H.R. Reiss, Phys. Rev. A **22**, 1786 (1980)
17. S. Borbély, K. Tőkési, L. Nagy, Phys. Rev. A **77**, 033412 (2008)
18. D.P. Dewangan, J. Eichler, Phys. Rep. **247**, 59 (1997)
19. D.M. Volkov, Z. Phys. **94**, 250 (1935)
20. R. Abrines, I.C. Percival, Proc. Phys. Soc. **88**, 861 (1966)
21. R.E. Olson, A. Salop, Phys. Rev. A **16**, 531 (1977)
22. D.G. Arbó, S. Yoshida, E. Persson, K.I. Dimitriou, J. Burgdörfer, Phys. Rev. Lett. **96**, 143003 (2006)